Journal of Pharmaceutical Innovation (2019) 14:159–175
https://doi.org/10.1007/s12247-018-9346-9

ORIGINAL ARTICLE

A Novel Stabilizing Approach to Improve the Manufacturing of Biodegradable Microparticles Entrapping Plasticizing Active Molecules: the Case of 4-Methoxychalcone

Danyela Francine Benvenutti[1] · Tania Mari Bellé Bresolin[1] · Rogerio Corrêa[1] · Stefano Giovagnoli[2] · Riccardo Vivani[2] · Maurizio Ricci[2]

Published online: 7 September 2018

Abstract

Purpose The microencapsulation of plasticizing molecules, such as 4-methoxy chalcone (4MC), can raise serious stability issues in microparticle (MP) manufacturing and storage, especially when employing low glassy pseudo-plastic polymers, such as polylactides (PLA) and polylactide-co-glycolides (PLGA). In this work, two distinct steps were undertaken: (1) the study of the effect on manufacturing and storage of 4MC loading in polyester MP and (2) the investigation of a new stabilization strategy based on 4MC intercalation into a stearate-modified hydrotalcite (sHTC).

Methods 4MC was loaded up to 20% *w/w* in PLA and PLGA MP by a W/O emulsion solvent extraction/evaporation method. Likewise, the 4MC-sHTC intercalation compound was prepared and loaded in the MP in the same conditions using a W/O/W double-emulsion method. All preparations were characterized by spectrophotometry, thermal analysis, x-ray powder diffraction (XRPD), scanning electron microscopy (SEM), and energy-dispersive x-ray spectroscopy (EDX) and for their particle size, in vitro drug release profile and kinetics. Storage stability was assessed over 8 months of incubation at room temperature (rt) and 30% relative humidity (RH).

Results The obtained 4MC-loaded MP showed a non-straightforward loading-dependent change of size, morphology, and release behavior. 4MC loading caused extensive clumping and poor MP recovery. Thermal and XRPD analyses confirmed a strong plasticizing effect of 4MC that, in some cases, segregated as crystals on the particle surface. Plasticization was inversely related to drug release. The loading of 4MC as a sHTC intercalation compound granted increased stability upon manufacturing and SEM-EDX evidenced a loading effect on porosity and the 4MC-sHTC distribution inside the MP. A remarkable stability increase was observed over 8 months storage at rt and 30% RH with no changes in the outer and inner MP morphology and compound distribution.

Conclusions The use of sHTC could be a useful stabilization strategy to improve manufacturing of biodegradable MP, surely worthy of further investigation in order to be extended to other MP drug delivery systems.

Keywords Chalcone · Biodegradable polymers · Plasticizing effect · Microparticles · Stearate-modified hydrotalcite

Introduction

Chalcones are a family of compounds characterized by an α,β-unsaturated ketone moiety [1]. These compounds are largely studied because of their broad spectrum of interesting biological activities. Chalcones have been associated with antibacterial [2, 3], antifungal [4, 5], antiviral [6], antimalarial [7, 8], anti-leishmania [9, 10], anti-inflammatory [11, 12], antiplatelet [13], antitumor [14, 15], antioxidant, and osteogenic effects [16, 17].

Among all, (2E)-1-phenyl-3-(4-methoxyphenyl)-2-propen-1-one (4MC) is particularly attractive in light of an

Electronic supplementary material The online version of this article (https://doi.org/10.1007/s12247-018-9346-9) contains supplementary material, which is available to authorized users.

✉ Stefano Giovagnoli
stefano.giovagnoli@unipg.it

✉ Maurizio Ricci
maurizio.ricci@unipg.it

[1] Center of Health Sciences, Universidade do Vale do Itajaí (UNIVALI), P.O. box 360, Itajaí, Santa Catarina 88302-202, Brazil

[2] Department of Pharmaceutical Sciences Università degli Studi di Perugia, Via del Liceo 1, 06123 Perugia, Italy

observed significant cytotoxicity against several tumor cell lines [18] and a very interesting activity as chemopreventor, chemosensitizer [19], as well as anti-inflammatory agent [20]. Nevertheless, such promising 4MC features reflect intrinsic issues, such as low water solubility and photosensitivity [21], that require suitable controlled release strategies in order to turn it into a valuable therapeutic agent. Therefore, microencapsulation could be helpful to develop effective delivery approaches for 4MC. In this regard, biodegradable polymeric microparticles (MP) represent a powerful tool in many different therapeutic areas, due to the possibility of controlling properties such as particle size, shape, inner structure, porosity, and drug loading, so as to obtain the desired drug release profile [22, 23]. Based on this principle, several administration routes, e.g., oral [24], intramuscular [25], intraperitoneal [26], intra-articular [27], pulmonary [28], and intranasal [29], can be exploited.

Unfortunately, a number of problems can affect MP formulations when small hydrophobic molecules, such as 4MC, are being loaded. Many of these issues relate to drug-polymer interaction [30] and are more often observed with low glassy pseudo-plastic polymers, such as polylactides (PLA) and poly(lactide-co-glycolides) (PLGA) [31]. These polymers are approved by the US Food and Drug Administration for parenteral use and have been explored as wall materials for a wide variety of pharmaceutical and biomedical applications, from drug targeting to depots and scaffolds for tissue engineering [32–36]. The most interesting aspect in the use of polyesters is the possibility to tailor drug release according to precise polymer properties, e.g., molecular weight (MW) and monomer composition, which change their biodegradation time profile [37]. However, for the above reasons, small entrapped molecules can dramatically alter thermal and mechanical properties of the particles as well as their release behavior. In addition, the plasticizing effect of small hydrophobic drugs is known to produce serious manufacturing issues, such as poor recovery upon preparation as well as limited storage stability [38]. Nevertheless, albeit the importance of these aspects that potentially hinder the development of such pharmaceutical forms, solutions in the field are lacking. Recently, cyclodextrins were employed to prevent ketoprofen-dependent plasticization of low MW polyester MP upon manufacturing by avoiding the physical interactions between the drug and the polymer chains [39]. Following this principle, in this work, we explored a potential novel stabilization approach in order to improve manufacturing and long-term storage of 4MC-loaded polyester MP. We proposed for the first time the use of a stearate (ST)-modified hydrotalcite (sHTC) anionic clay. These hydrophobically modified clays have been employed as fillers to improve mechanical, thermal, and gas permeability properties of polymers [40], but, to the best of our knowledge, they have never been explored as stabilizers in pharmaceutical formulations.

The large interlayer spacing and modified environment of sHTC can allow intercalation of hydrophobic small molecules that, not bearing the proper functional groups, like 4MC, cannot give rise to the ion exchange process required for binding in conventional HTC. Thus, such molecules can accommodate in the sHTC hydrophobic pocket in light of their affinity. This may simplify the intercalation procedure that can occur by a simple solvent-free physical guest-host contact. Such features may also grant high intercalation payloads.

The study was conducted in two steps: step (1) being the first time that 4MC is encapsulated in polyester MP, the effect of 4MC loading on several PLA, and PLGA MP batches was addressed by measuring MP properties, release behavior, and kinetics; step (2) the use of sHTC was explored determining MP properties upon manufacturing and long-term storage. Albeit preliminary, if successful, this approach may be proposed for a number of different manufacturing techniques and delivery systems.

Materials and Methods

Materials

4MC was synthesized by Claisen-Schmidt condensation, as reported elsewhere [41], with a yield of 83%. Structure and purity were confirmed by ^{1}HNMR, ^{13}CNMR, and gas chromatography-mass spectrometry analyses. Poly(DL-lactide-co-glycolide) (75:25), inherent viscosity 0.76 dL/g, MW 66–107 kDa, and 1.1–1.54 g/cm^3 density (PDLG7507); poly(D,L-lactide-co-glycolide) (50:50) acid terminated, MW 38–54 kDa and 0.45–0.60 dL/g inherent viscosity (Resomer® RG504H); poly(D,L-lactide-co-glycolide, 50:50), ester terminated, MW 38–54 kDa, 0.45–0.60 dL/g inherent viscosity (Resomer® RG504); Poly (D,L-lactide-co-glycolide) (50:50), ester terminated, MW 7–17 kDa, 0.16–0.24 dL/g inherent viscosity (Resomer® RG502); poly(D,L-lactide-co-glycolide) (50:50), carboxylic acid terminated, MW 40 kDa, 0.4 dL/g inherent viscosity (PDLG5004A 50:50); poly(D,L-lactide) acid terminated, MW 10–18 kDa, 0.16–0.24 dL/g inherent viscosity (Resomer® R202H); poly(D,L-lactide) ester terminated, MW 10–18 kDa, 0.16–0.24 dL/g inherent viscosity (Resomer® R202S), were purchased from PURASORB® (PURAC biochem, Gorinchem, the Netherlands) and Boerhinger Ingelheim (Milan, Italy). Polyvinyl alcohol (PVA, MW 30 kDa) was purchased from Sigma-Aldrich (Milan, Italy) and polyethylene glycol 400 (PEG400) from Farmalabor srl (Milan, Italy). All other chemicals and reagents were of the highest purity grade commercially available.

Microparticle Preparation

Microparticles loaded with 4MC were prepared by an O/W emulsion solvent extraction/evaporation method. Briefly, a 0.1% *w/v* PVA water solution was employed as continuous phase. The oil phase was prepared by dissolving an appropriate amount of 4MC and polymer in dichloromethane. The polymers chosen were PDLG7507, Resomer® RG504H, Resomer® RG504, Resomer® RG502, PDLG5004A, Resomer® R202H, and Resomer® R202S. The MP were loaded with 5, 10, and 20% *w/w* 4MC and the inner/outer phase ratio in the emulsion was 1:100 *v/v*. Solvent evaporation was performed according to the following temperature/stirring program: 4 °C for 5 min, 25 °C for 1 h, 30 °C for 1 h, 40 °C for 30 min, and 15 °C for 10 min. Stirring was maintained at 600 rpm throughout the process. The microparticles were harvested by filtration under nitrogen pressure at room temperature (rt) through a 5-μm nitrocellulose filter (Millipore, Milan, Italy). Three consecutive washing cycles were carried out with ultrapure water. The MP were vacuum-dried for 24 h at rt.

Preparation of 4MC-sHTC Intercalation Compound

4MC was included in the interlayer region of an Mg–Al sHTC clay. First, the Mg–Al HTC exchanged with $CH_3(CH_2)_{16}CO_2^-$ ST anions, up to 75% of the ion exchange capacity of the host, was prepared as described previously [42]. The final sHTC had the following composition: $Mg_{0.67}Al_{0.33}(OH)_2$ $ST_{0.248}(NO_3)_{0.082}{\cdot}0.5H_2O$ as determined by thermogravimetric analysis.

Portions of 1 g of this compound were then intimately mixed with 1 g of solid 4MC by gently grinding them in an agate mortar, for about 10 min. The solid mixture was then incubated at 80 °C for 5 days in an oven. After that, the final compound was stored in a closed vessel at rt, protected from light. X-ray powder diffraction (XRPD) and ^{1}HNMR analysis were performed to confirm successful intercalation of intact 4MC.

Preparation of 4MC-sHTC-Loaded Microparticles

In order to investigate the effect of 4MC intercalation in sHTC on MP manufacturing and storage, the intercalation compound was loaded at the same theoretical loading employed for the 4MC-loaded MP. A W/O/W double-emulsion solvent extraction/evaporation method was used following the same procedures and conditions described earlier. A weighed amount of 4MC-sHTC was dispersed thoroughly in water and mixed by vortexing in a dichloromethane polymer solution at 1:10 *v/v* ratio to form a W/O emulsion. The emulsion was transferred dropwise into a second 0.1% *w/v* PVA water solution, stirred at 600 rpm, at 1:100 *v/v* ratio. The same temperature program was employed to evaporate the organic solvent and, after hardening, the MP were recovered by filtration under nitrogen pressure and washed three times with ultrapure water. Vacuum drying was then performed for 24 h.

Microparticle Characterization

Thermal behavior of the MP was evaluated by differential scanning calorimetry (DSC) using a Mettler Toledo DSC 821 calorimeter (Mettler Toledo, Switzerland) equipped with a liquid nitrogen cooling system. The system was calibrated using an indium standard. The MP samples were compared with free 4MC and blank MP.

The effect of 4MC on the polymer glass transition temperature (T_g) was evaluated on a set of samples prepared as described hereinafter. Amounts of 5 mg of each sample were exactly weighed and hermetically sealed in 40-μL pin-holed lid aluminum pans. The samples were subjected to two heating cycles: from 15 to 90 °C and − 5 to 85 °C, at 5 °C/min, in triplicate. T_g was determined as the inflection point of the sigmoidal transition on the second heating ramp in order to erase sample thermal history. The obtained DSC data were treated with STARe software.

Morphological characteristics, surface and porosity were investigated by scanning electron microscopy (SEM) using a FEG LEO 1525 scanning electron microscope (Bruker, Milan, Italy). Samples were prepared by placing the MP powder onto an aluminum specimen stub covered with a double-sided carbon adhesive disc. The samples were sputter-coated with chromium prior to imaging. Coating was performed at 20 mA for 25 s. Energy-dispersive x-rays spectroscopy (EDX) was performed to determine the 4MC-sHTC distribution in the MP. The Mg and Al signals inside and on the surface of the MP were measured at 15 kV with acquisition times of 20 min. Coating was performed with graphite at 20 mA for 22 s.

X-ray powder diffraction patterns were collected according to the step scanning procedure with the PANalytical X'Pert Pro, Cu Ka radiation diffractometer, operating at 40 kV and 40 mA. The powders were deposited in a shallow well of a sample holder. Prior to analysis, a slightly rough flat surface was used to press down the powder, packing it into the well to minimize preferred orientation.

To determine MP size distribution, an Accusizer C770 (PSS Inc., Santa Barbara, CA, USA) based on the "single particle optical sensing" technique and equipped with an autodilution system was used. The MP were suspended in deionized water before analysis. Analyses were performed in triplicate and the size was expressed as volume mean diameter (d_{mv}). Population span was calculated according to Eq. (1),

$$\text{Span} = \frac{d_{90} - d_{10}}{d_{50}} \quad (1)$$

where d_{10}, d_{50}, and d_{90} are the particle diameters at 10, 50, and 90%, respectively, of the population distribution calculated from the sample.

Drug content (%DC, Eq. 2) and loading efficiency (%LE, Eq. 3) were measured by spectrophotometry, using an Agilent 8453 UV-Vis spectrophotometer equipped with a Peltier temperature controller.

$$\%\mathrm{DC} = \frac{\text{Amount of entrapped drug}}{\text{MP weight}} \times 100 \quad (2)$$

$$\%\mathrm{LE} = \frac{\text{measured drug loading}}{\text{theoretical drug loading}} \times 100 \quad (3)$$

4MC extraction from the MP was performed by dissolving a weighed amount of the MP in a 1:4 *v*/*v* acetonitrile-methanol solution. The obtained solution/dispersion was centrifuged at 3400 rpm for 15 min at rt. After centrifugation, 1 mL of supernatant was diluted in methanol and submitted to UV-Vis analysis. All measurements were performed in triplicate and the results expressed as mean ± SD. A calibration curve of 4MC in methanol was built in the 2–20 μg/mL concentration range (λ_{max} = 346 nm, r^2 = 0.9991).

In Vitro Drug Release

In vitro drug release experiments were performed by the dialysis bag method. In order to ensure sink conditions throughout the experiment, a 30% *w*/*v* PEG400 in 0.1 M phosphate buffer pH 7.4 solution was employed as release medium. Briefly, a weighed amount of the MP was dispersed in the release medium and placed in a dialysis bag (12–14 kDa MWCO). The bag was sunk in a 50-mL conical Falcon tube and incubated at 37 °C. At predetermined time intervals, aliquots were withdrawn and replaced with fresh release medium maintained at 37 °C. Drug release quantification was performed by UV-Vis spectrophotometry using the method described above. All measurements were performed in triplicate and the results expressed as mean ± SD.

Drug Release Kinetics

Classical models were employed to investigate 4MC release mechanism from the MP and to address the effect of 4MC-sHTC loading [33]:

(a) The Higuchi model (Eq. 4) is one of the most popular to study pure Fickian transport, although limited to one-dimensional diffusion from planar surfaces [43]:

$$M_t = \mathrm{A}\sqrt{D(2C_0 - C_s)t} \quad (4)$$

where M_t is the drug cumulative amount released at time t, t is the time, A is the surface area, D is the diffusivity of the drug through the matrix, and c_0 and c_s are the initial drug concentration and drug solubility, respectively.

(b) The power law, a general case of the Higuchi model (n = 0.5), referred to as the Peppas' equation (Eq. 5) [44]:

$$\frac{M_t}{M_\infty} = \mathrm{k}t^n \quad (5)$$

where M_∞ is the drug amount released at infinity, k is the experimental parameter, and n is the coefficient depending on the geometry of the system and correlated to the release mechanism.

(c) For n approaching 1, the mechanism is shifted towards a case II transport [45] and Eq. 5 turns into a zero-order kinetics (Eq. 6).

$$\frac{M_t}{M_\infty} = \mathrm{k}t \quad (6)$$

Lack of fit was evaluated by applying a Levenberg-Marquardt method for the minimization of the reduced χ^2 function [46, 47].

Storage Stability of 4MC-Loaded MP

Storage stability of the 4MC and 4MC-sHTC MP was evaluated by SEM, EDX, DSC, and XRPD analyses. Changes in morphology and drug physical state were determined on 20% *w*/*w* loaded MP over 8 months of storage at rt and 30% relative humidity (RH). Samples for SEM, DSC, and XRPD analyses were prepared as described above.

Statistical Analysis

Glass transition data were analyzed for statistical difference by one-way ANOVA and one-way ANOVA on ranks applying the Dunnet and Holm-Sidak multiple comparison post-hoc methods to determine differences against a blank MP reference group at 95% significance level.

Results and Discussion

Step 1. Effect of 4MC Loading on Polyester MP

4MC Loading Effect on MP Properties

The characteristics of the obtained 4MC-loaded MP are displayed in Table 1. The total yield of the preparation process ranged between 43 and 99%, with %LE between 56 and 100%. A loading-dependent %LE reduction was observed

Table 1 Properties of 4MC-loaded biodegradable MP obtained at different drug loading

Polymer	Blank		5%				10%				20%			
	d_{mv} (μm) (SD)	Span	d_{mv} (μm) (SD)	Span	DC (%) ± SD	LE (%) ± SD	d_{mv} (μm) (SD)	Span	DC (%) ± SD	LE (%) ± SD	d_{mv} (μm) (SD)	Span	DC (%) ± SD	LE (%) ± SD
PDLG7507	81.3 (37.1)	1.18	84.4 (38.2)	1.08	4.1 ± 0.6	82.2 ± 6.1	71.3 (32.2)	1.19	8.6 ± 0.1	85.5 ± 7.6	82.9 (36.3)	1.11	17.3 ± 0.9	86.3 ± 9.3
RG504H	55.2 (25.1)	1.47	59.2 (24.0)	1.07	3.7 ± 0.9	74.2 ± 9.4	54.0 (24.2)	1.20	8.6 ± 0.3	85.7 ± 3.3	288.7 (113.23)	1.03	19.6 ± 1.6	98.2 ± 15.7
RG504	67.7 (34.1)	1.50	59.9 (27.2)	1.26	4.2 ± 0.6	84.1 ± 6.2	54.5 (26.7)	1.45	4.6 ± 1.4	46.2 ± 13.6	108.9 (66.8)	1.72	12.4 ± 1.1	61.5 ± 11.1
RG502	78.1 (39.9)	1.36	65.6 (26.2)	1.04	4.2 ± 0.5	84.2 ± 5.2	54.9 (22.8)	1.10	9.0 ± 0.8	90.1 ± 7.6	67.2 (30.9)	1.13	19.3 ± 1.3	96.6 ± 13.5
PDLG5004A	50.5 (21.0)	1.19	62.5 (25.3)	1.09	4.4 ± 0.4	87.9 ± 4.3	65.8 (27.4)	1.06	10.0 ± 0.7	100.0 ± 7.0	79.1 (32.9)	1.04	19.9 ± 1.7	99.3 ± 17.2
R202H	67.3 (23.3)	0.87	72.3 (26.3)	1.01	3.9 ± 0.7	78.8 ± 6.9	71.5 (28.4)	0.83	10.1 ± 1.1	100.6 ± 10.8	91.8 (58.4)	1.85	18.7 ± 2.6	93.6 ± 26.1
R202S	67.9 (25.3)	0.92	74.2 (21.1)	0.77	4.3 ± 0.1	85.6 ± 1.5	109.1 (61.1)	1.64	6.6 ± 1.4	65.7 ± 13.7	64.2 (41.3)	2.41	11.3 ± 1.1	56.4 ± 11.5

for the endcapped polymers RG504 and R202S, while their non-endcapped counterparts, RG504H and R202H, showed an opposite behavior, with %LE and %DC increasing with loading. All the other formulations showed a more consistent behavior, with %LE values > 80%. Drug content varied accordingly between 3.7 and 4.4% at 5, 4.6, and 10% at 10% and 11 and 20% at 20% *w*/*w* 4MC loading. These findings highlight a high affinity of 4MC for PLA and PLGA matrices as proved by the nearly complete drug recovery measured for most formulations.

Particle size (Supplementary Fig. 1) and morphological analysis (Fig. 1) were generally in agreement, confirming a smaller size, ranging between 50 and 80 μm, at 5% *w*/*w* loading and a sensible increase with loading. The largest MP were recorded for RG504H and RG504 polymers and reached a d_{mv} of 109 and 288 μm, respectively. Such an increase was not accompanied by a significant *span* increase (1.03 and 1.72, respectively). In turn, span reached values up to 1.85 and 2.41 at 20% *w*/*w* loading for the R202H and R202S MP, respectively, indicating aggregation phenomena.

In particular, the R202S MP resulted not only aggregated but also irregularly clumped into large fused blocks (Fig. 1D) and fused particles were observed even at lower 4MC loadings (Fig. 1C). Considerable deformation and random cracking was observed for the RG502 and PDLG5004A MP at 20% *w*/*w* loading (Fig. 1N, n).

These effects clearly suggest polymer plasticization and then annealing due to 4MC. Such a phenomenon is well documented for small hydrophobic molecules, including several drugs [31, 37]. In particular, the effect on the R202S MP demonstrates that the formulation of drug-loaded biodegradable MP can be almost completely hindered by loading of small hydrophobic molecules, like 4MC, into low glassy plastic polymers. Such a phenomenon inevitably reflects a likely storage instability as well [36]. In part, the extent of this effect depends on the polymer hydrophobicity, which determines the affinity between the matrix and the entrapped molecules [48, 49].

Since hydrophobicity increases with endcapping and MW, 4MC loading affected less the R202H polymer than the R202S one, while the larger 50–50 PLGA polymers, such as RG504H, RG502, and PDLG5004A, were significantly perturbed. An exception to this behavior is PDLG7507 that, although more hydrophobic, showed higher resistance to annealing, likely due to a higher glassy state (Fig. 1O–R).

Thermal analysis confirmed the previous hypothesis of extensive polymer plasticization upon 4MC loading (Table 2, Supplementary Fig. 2). A significant loading-dependent linear shift from an anti-plasticizing to a plasticizing effect was recorded for the RG502 and, particularly, RG504H MP ($p < 0.05$). The RG504 and PDLG5004A MP were the least affected ($p > 0.05$).

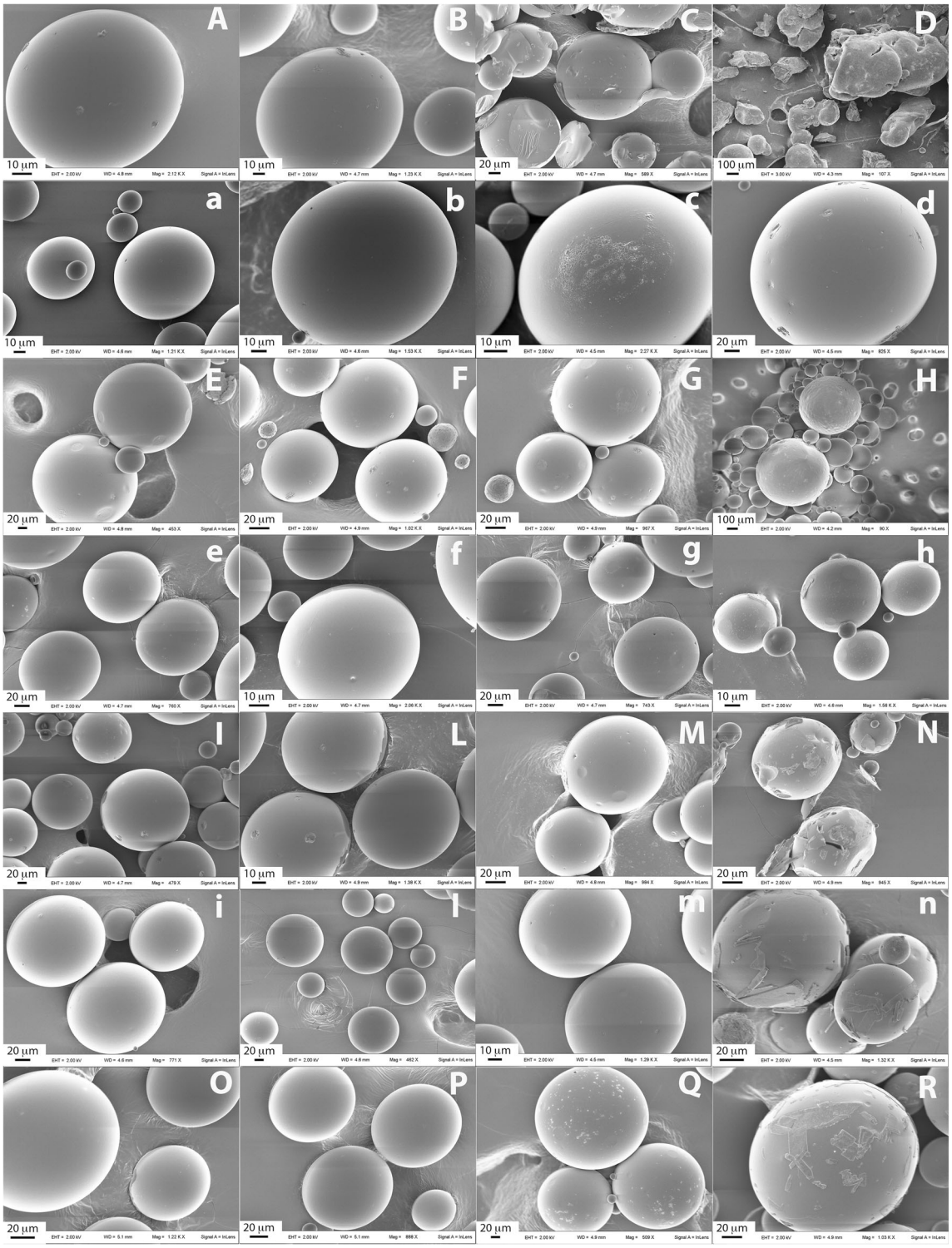

Fig. 1 Comparison of MP morphology at, from left to right, 0, 5, 10, and 20 *w*/*w* 4MC loading. **A**–**D** R202S. **a**–**d** R202H. **E**–**H** RG504H. **e**–**h** RG504. **I**–**N** RG502. **i**–**n** PDLG5004A. **O**–**R** PDLG7507

A significant anti-plasticizing effect was recorded for the RG504H MP at 5 and 10% *w*/*w* loading ($p < 0.05$), which turned into a remarkable plasticization, producing a T_g drop of − 17 °C at 20% *w*/*w* loading ($p < 0.05$). The PDLG7507 MP were significantly plasticized at all loadings, while the R202S MP showed the strongest plasticization with about − 23 °C T_g drop. This behavior can explain the poor recovery for this MP formulation.

XRPD analysis (Fig. 2) as well as DSC profiles (Supplementary Fig. 2) provided evidence of the presence of

Table 2 Thermal analysis of 4MC-loaded MP. Glass transition temperature values at different 4MC loading and T_g change compared to blank MP

Polymer	Blank	5%		10%		20%	
	T_g ± SD	T_g ± SD	ΔT_g	T_g ± SD	ΔT_g	T_g ± SD	ΔT_g
PDLG7507	41.7 ± 3.1	32.4 ± 2.8	− 9.3**	33.3 ± 0.5	− 8.4**	27.4 ± 0.5	− 14.3**
RG504H	24.5 ± 0.6	33.1 ± 2.4	+8.6**	28.4 ± 3.2	+3.9**	7.6 ± 0.6	− 16.9**
RG504	25.9 ± 0.5	28.1 ± 0.6	+2.2	24.6 ± 0.5	− 1.2	26.8 ± 1.8	+0.9
RG502	29.1 ± 2.8	31.7 ± 1.3	+2.6	31.3 ± 1.0	+2.2	25.62 ± 0.05	− 3.5**
PDLG5004A	29.6 ± 2.8	27.4 ± 4.2	− 2.3	29.8 ± 2.2	+0.2	26.5 ± 1.2	− 3.1
R202H	44.7 ± 5.6	30.0 ± 1.4	− 14.7**	40.8 ± 3.5	− 3.9	28.5 ± 1.2	− 16.2**
R202S	39.2 ± 2.0	41.1 ± 1.8	+1.9	30.3 ± 0.7	− 9.0**	16.5 ± 2.2	− 22.8**

$\Delta T_g = T_g$ loaded $- T_g$ blank

$^{**}p < 0.05$ compared to blank

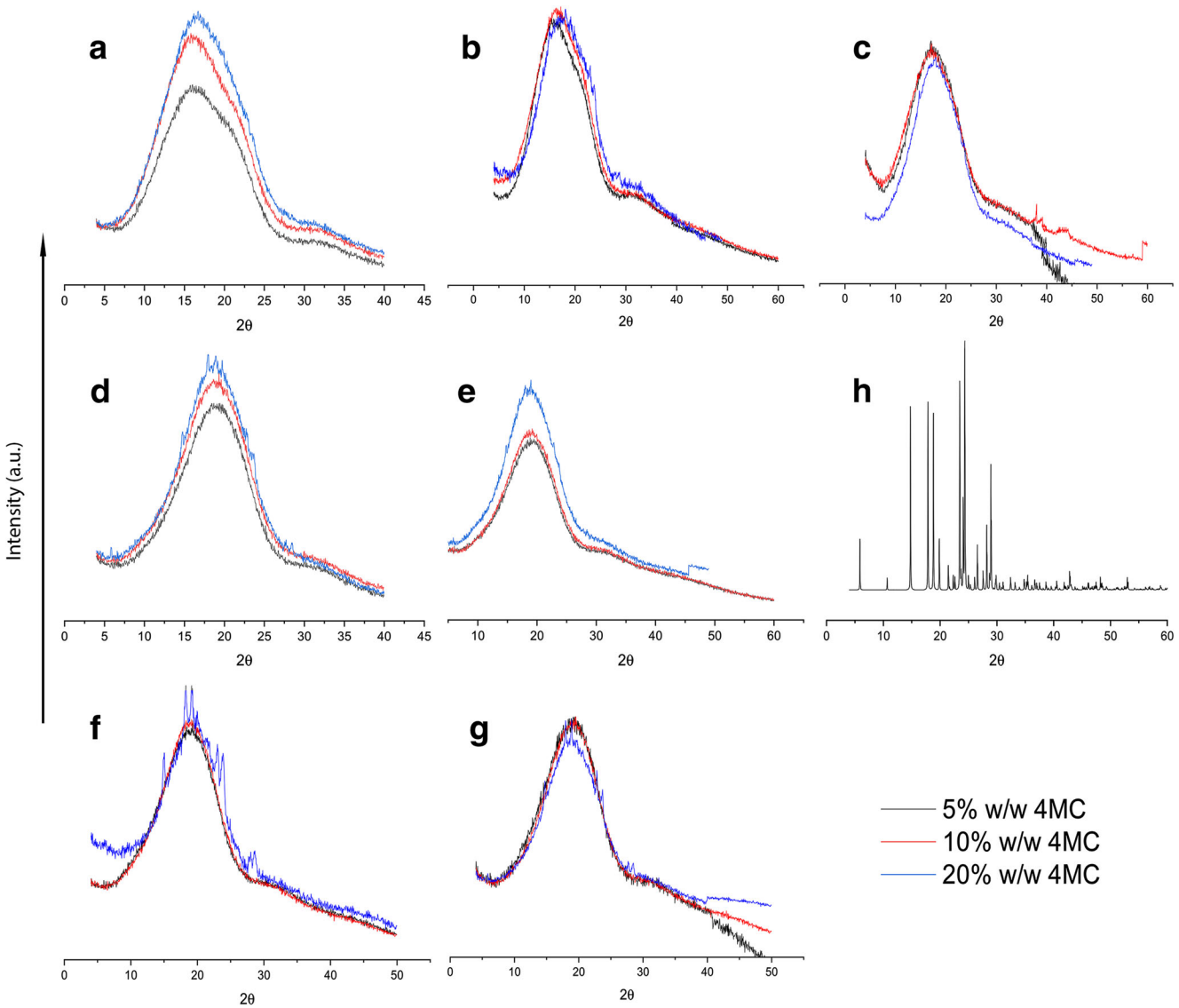

Fig. 2 XRPD profiles of 4MC-loaded MP. **a** R202H. **b** R202S. **c** PDLG7507. **d** RG502. **e** RG504. **f** RG504H. **g** PDLG5004A. **h** XRPD profile of crystalline 4MC

small typical signals of crystalline 4MC at 20% *w/w* loading, in particular for the RG504H, PDLG5004A, R202S, and RG502 MP (Fig. 2d–h). These findings correlate with the segregation of excess 4MC on the surface of the particles, in agreement with the morphological observations.

4MC Loading Effect on In Vitro Release Profiles

Drug release from polymeric MP is generally known to decrease with polymer MW and to increase with drug loading and polymer plasticization [50, 51]. Accordingly, the 4MC release generally increased with loading up to completion, especially for the RG504, RG502, PDLG5004A, and R202H MP (Fig. 3a–c). Such a behavior may, in part, correlate with the observed 4MC segregation on the particle surface when loading increased. On the other hand, the observed clumping and fusion of the R202S MP and, to a lower extent, the size increase of the RG504H MP at 20% *w/w* loading sensibly slowed down the respective releases (Fig. 3c). Moreover, a prevalent effect of the high MW and hydrophobicity of PDLG7507 determined a low release independently of loading, plasticization, and 4MC segregation (Fig. 3a–c).

A non-canonical correlation between polymer plasticization and drug release was observed as well. In fact, an inverse and almost linear relationship connected ΔT_g and drug release, especially at 20% *w/w* loading ($r^2 = 0.87907$, Supplementary Fig. 3), suggesting that the increase in polymer plasticization due to 4MC loading reduced drug release.

This behavior may be understood considering that in the case of low T_g shear thinning materials, such as PLA and PLGA polymers, the effect of the long-term exposure to temperatures close to T_g can cause annealing of the solid matrices that may then result less porous, more deformable, and with a homogeneous texture [52]. This is the case of the obtained 4MC-loaded MP that were non-porous and with a continuous core regardless of the polymer employed (Supplementary Fig. 4). This inner homogeneity and lack of pores, often observed for plasticized PLGA MP [53, 54], may have determined the inverse relationship between release rate and plasticization.

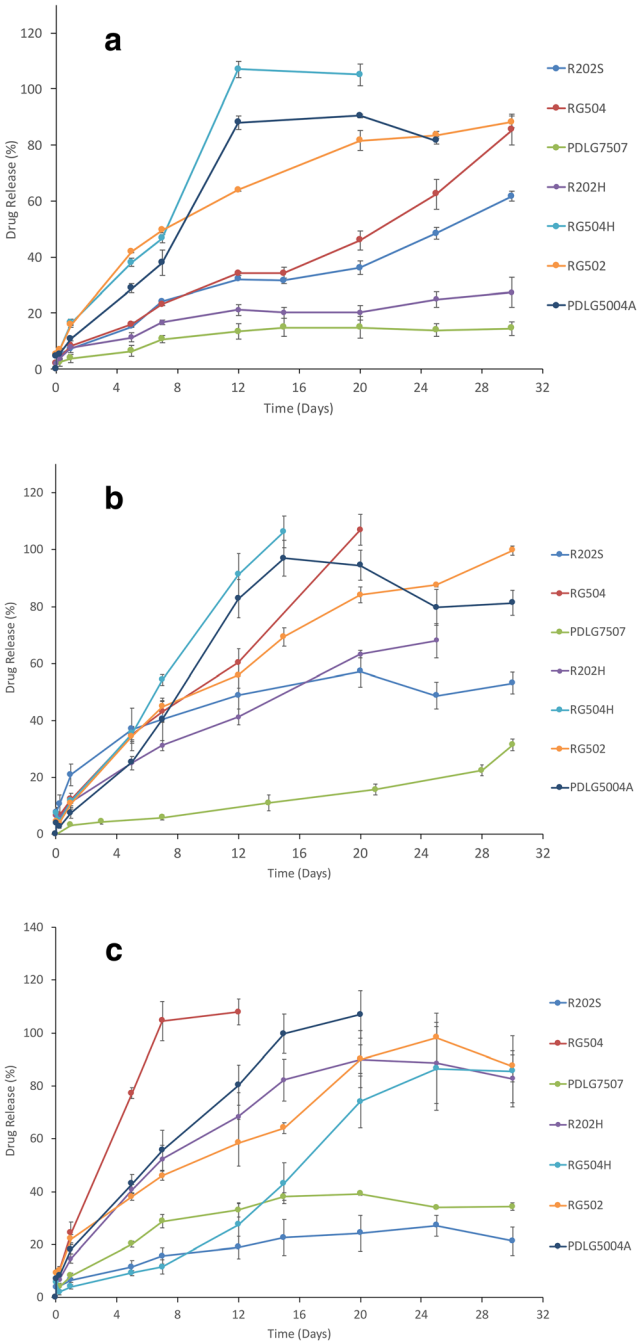

Fig. 3 In vitro release profiles of the 4MC-loaded MP over a 30-day period. **a** 5%, **b** 10%, and **c** 20% *w/w* 4MC loading. The experiment was performed in triplicate in 30% *w/v* PEG400, 0.1 M phosphate buffer pH 7.4 at 37 °C

Release Kinetics

In order to better understand the underlying release kinetics and prevalent release processes, the obtained profiles were fitted to the Higuchi's, Peppas', and zero-order kinetic models (Eq. 4–6, Table 3). These models show limitations arising from the assumptions at the origin of their mathematical derivation, which restrict their application to complex systems, such as biodegradable polymeric MP. Therefore, in this work, cautious interpretation of the fitting results is required, thus accounting for significant mismatch between the proposed and actual release mechanisms. Nevertheless, their simplicity was useful to allow comparison of contingent changes in the release processes among the different MP formulations.

As expected, the Peppas' model (Eq. 5) fitted better the experimental data than the Higuchi's or zero-order kinetic models (Table 3). This is a consequence of its better compliance with mass transport processes in particulate systems, for

Table 3 Fitting comparison of zero-order, Higuchi's, and Peppas' models to 4MC in vitro release data from biodegradable polyester MP

Model		Zero order		Higuchi		Peppas		
Polymer	% *w/w* loading	Adj. r^2	Red. χ^2	Adj. r^2	Red. χ^2	Adj. r^2	Red. χ^2	$n \pm$ (SE)
R202S	5	0.93566	26.03	0.94355	22.84	0.96754	13.14	0.69 ± 0.07
	10	0.31446	308.88	0.80750	86.73	0.94453	24.99	0.28 ± 0.04
	20	0.57485	37.79	0.89985	8.90	0.93912	5.41	0.35 ± 0.05
R202H	5	0.68301	29.31	0.95217	4.42	0.97531	2.28	0.38 ± 0.04
	10	0.91631	52.93	0.97736	14.32	0.98736	7.99	0.60 ± 0.04
	20	0.71833	369.72	0.95072	64.68	0.95761	55.65	0.43 ± 0.06
RG502	5	0.78798	258.74	0.98739	15.39	0.99103	10.94	0.45 ± 0.03
	10	0.90918	124.14	0.98662	18.29	0.99414	8.00	0.59 ± 0.03
	20	0.80597	237.34	0.96392	44.14	0.96440	43.55	0.48 ± 0.06
RG504H	5	0.89992	212.22	0.91090	188.94	0.93322	141.62	0.67 ± 0.13
	10	0.99029	16.56	0.91400	146.69	0.99083	15.65	0.91 ± 0.07
	20	0.89385	109.32	0.77327	233.51	0.88224	121.28	0.98 ± 0.21
RG504	5	0.97138	21.37	0.87195	95.61	0.96822	23.73	0.99 ± 0.10
	10	0.97760	34.49	0.88341	179.47	0.97584	37.19	0.92 ± 0.10
	20	0.85187	408.10	0.97234	76.22	0.97241	76.02	0.51 ± 0.07
PDLG5004A	5	0.80973	276.28	0.89126	157.90	0.89660	150.15	0.57 ± 0.13
	10	0.70183	488.15	0.85191	242.45	0.85193	242.41	0.50 ± 0.13
	20	0.96038	74.90	0.96997	56.76	0.99416	11.04	0.69 ± 0.04
PDLG7507	5	0.22668	19.86	0.73034	6.93	0.78947	5.41	0.36 ± 0.09
	10	0.97663	2.72	0.84177	18.39	0.97344	3.09	1.05 ± 0.12
	20	0.29836	134.59	0.79337	39.64	0.86320	26.24	0.34 ± 0.08

Adjusted r^2 r^2 adjusted for the number of predictor terms in the model, *Reduced* χ^2 χ^2/DoF as obtained by the Levenberg-Marquardt method

which a physical meaning of the n coefficient value has been defined [55, 56]. In particular, for spherical particles, $n \leq 0.43$ has been linked to a pure Fickian transport, $0.43 < n < 0.85$ to a diffusion and case II transport combined mechanism, referred to as anomalous transport, $n \geq 0.85$ to a case II transport, and $n = 1$ to a zero-order kinetics.

Generally, diffusive processes seemed to prevail as MP plasticization and size increased (Supplementary Fig. 5). For the RG504 and R202S MP, an increase in drug loading caused a shift from an anomalous to case II transport or to pure Fickian transport. A more consistent behavior, almost independent of loading, was observed for the R202H, RG502, and PDLG5004A MP that showed a predominant pure Fickian diffusion mechanism ($0.38 < n < 0.60$) and a Fickian diffusion case II transport combined mechanism ($0.45 < n < 0.69$), respectively. The PDLG7507 MP followed a pure Fickian diffusion mechanism at 5 and 20% *w/w* loading ($n = 0.36, 0.34$), while the release approached a zero-order kinetics at 10% *w/w* loading ($n = 1.14$). Overall, 4MC loading resulted critical in influencing the release process as a result of the strong MP plasticization. Therefore, a logical impact on MP storage should be expected.

Step 2. sHTC Intercalation Compounds as a Strategy to Prevent MP Manufacturing Problems

Considering the remarkable effect of 4MC loading on all batches and, in particular, on the R202S MP, this formulation was selected to explore the effect of 4MC intercalation in sHTC clay on MP manufacturing and storage. The starting hypothesis is that the intercalation in sHTC may prevent the observed issues by avoiding direct contact of the active molecule with the polymer.

In order to achieve this goal, innovative approaches were applied to allow 4MC loading in sHTC lamellar clays. In fact, 4MC is highly hydrophobic and it is devoid of the negative charge needed for the binding with the positively charged HTC layers. Therefore, HTC was modified with ST to form a hydrophobic pocket able to accommodate 4MC in high amounts. In this way, it was possible to obtain a > 50% *w/w* 4MC-sHTC compound. The intercalation compound was obtained as above described and had the following composition: $Mg_{0.67}Al_{0.33}(OH)_2$ $ST_{0.248}(NO_3)_{0.082}(4MC)_{0.56}$.

XRPD patterns (not shown) displayed an increased basal spacing from 30.5 Å interlayer distance of sHTC to about 38 Å. At the same time, the typical peaks of crystalline 4MC were absent, likely attesting that 4MC was entrapped within the hydrophobic space generated by the intercalated ST. ^{1}HNMR measurements on 4MC extracted from sHTC with ethanol confirmed the structural preservation of the molecule upon intercalation (not shown).

The obtained 4MC-sHTC intercalation compound was then loaded in the R202S MP by a W/O/W double-emulsion solvent extraction/evaporation method. A change in the preparation method was required due to incompatibility between the O/W emulsion method previously employed and the intercalation compound. In fact, direct dispersion of 4MC-sHTC in dichloromethane would lead to extraction of 4MC from the clay. Therefore, the intercalation compound was first dispersed in water, emulsified in the organic polymer solution, and then dispersed in a second water phase with a stabilizer. Such a procedure should ensure reduced contact of the compound with the organic solvent thus avoiding leaching of 4MC from the clay.

The characteristics of the obtained MP are reported in Table 4. Particle size resulted increased compared to the MP previously obtained at 5 and 10% *w*/*w* loading, but much lower at 20% *w*/*w* loading. Drug content was generally comparable to that reported in Table 1 and consistent with the loading increase (%LE between 60 and 80%). The most important finding is the dramatic reduction of plasticization at 20% *w*/*w* loading, with a maximum T_g depletion of only about − 5 °C compared to the − 23 °C measured for the 4MC loaded R202S MP (see Table 2).

Particle size distributions were generally more homogeneous, especially at 20% *w*/*w* loading, with the presence of a few aggregates only at 5% *w*/*w* loading (Fig. 4a, left). The MP maintained their spherical shape, showing a loading-dependent porosity increase and consequently a rough surface (Fig. 4). The reason for such a morphology can be understood looking at the outer and inner MP structures (Fig. 4a, right). The double-emulsion method produced MP with internal cavities that represent the space previously occupied by the organic droplets and smaller inner water droplets. As a consequence, at 20% *w*/*w* loading, the MP appeared with a heterogeneous void core responsible for the observed surface roughness and porosity.

The 4MC-sHTC distribution in the MP resulted dependent on loading (Fig. 4b). The compound was denser in the particle core at 5% and, to a lower extent, at 10% *w*/*w* loading, whereas it distributed evenly inside and outside the MP at 20% *w*/*w* loading (Fig. 4c).

Table 4 Properties and effect on T_g values for 4MC-sHTC loaded MP at different drug loadings

Polymer	Blank		5%				10%				20%			
	d_{mv} (μm) (SD)	Span	d_{mv} (μm) (SD)	Span	DC (%) ± SD	LE (%) ± SD	d_{mv} (μm) (SD)	Span	DC (%) ± SD	LE (%) ± SD	d_{mv} (μm) (SD)	Span	DC (%) ± SD	LE (%) ± SD
R202S	49.6 (28.3)	1.61	98.6 (49.8)	1.01	3.4 ± 0.3	68.2 ± 2.8	122.4 (49.7)	1.00	8.0 ± 0.5	80.3 ± 5.4	61.5 (28.0)	1.24	12.2 ± 0.5	60.9 ± 5.4
	T_g ± SD		T_g ± SD		ΔT_g		T_g ± SD		ΔT_g		T_g ± SD		ΔT_g	
	41.4 ± 0.4		38.3 ± 1.0		− 3.0**		39.1 ± 0.2		− 2.2**		36.2 ± 0.6		− 5.2**	

$\Delta T_g = T_g$ loaded $- T_g$ blank

**$p < 0.05$ compared to blank

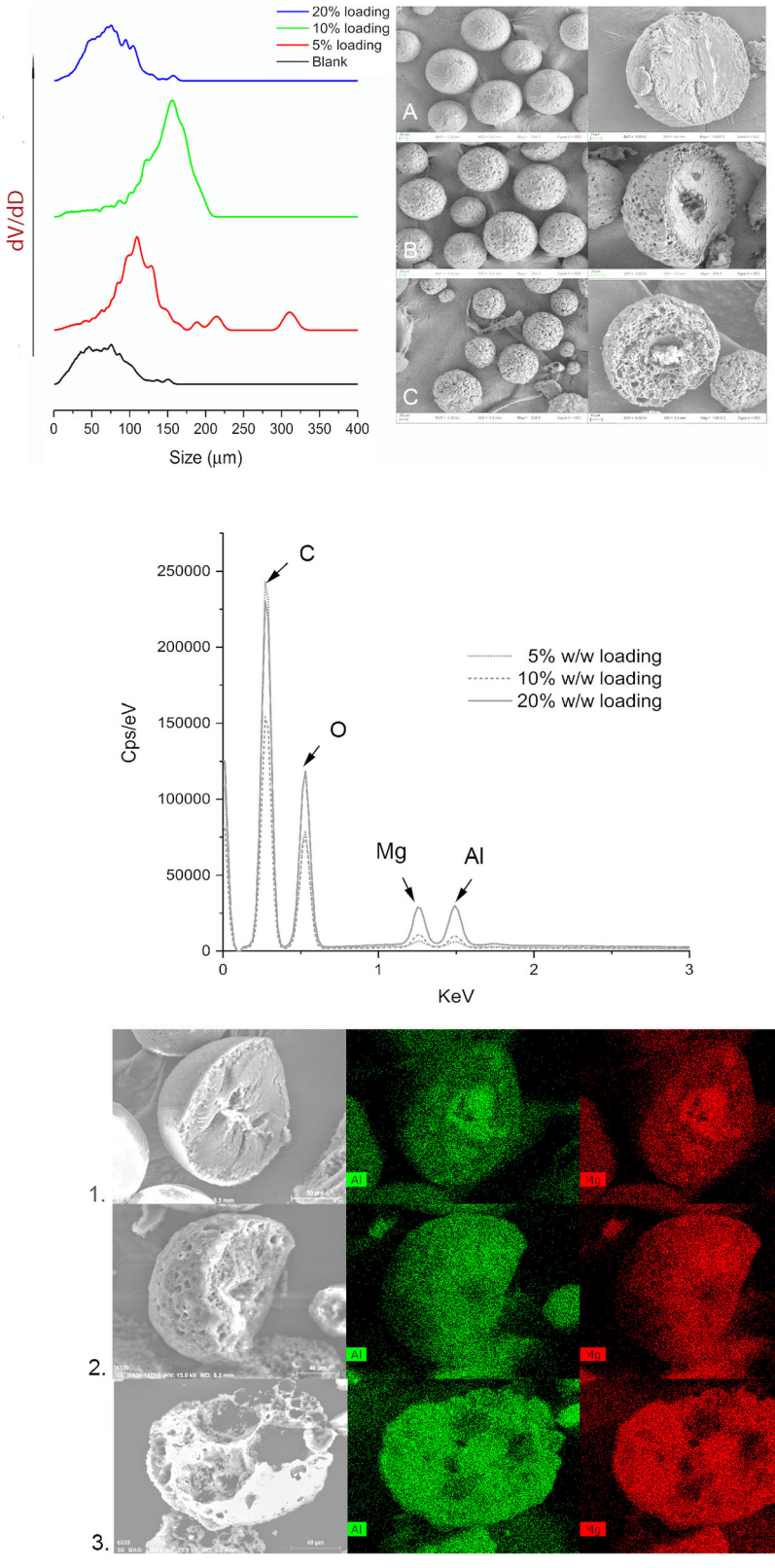

Fig. 4 **a** Comparison of particle size distribution (left) and outer and inner morphology (right) of the R202S MP loaded with 4MC-sHTC at A = 5%, B = 10%, C = 20% *w/w*. **b** EDX spectrum showing the loading-dependent signals of the Mg and Al components of sHTC. **c** EDX mapping of 4MC-HTCs distribution inside and outside the MP at 1 = 5%, 2 = 10% and 3 = 20% loading (red = Mg signal, green = Al signal)

The thermal and XRPD analyses revealed the presence of 4MC melting signals at 10 and 20% w/w loading (Fig. 5a). The DSC profiles correlated with the XRPD profiles showing small peaks at 20% *w/w* loading, likely ascribable to a small amount of crystalline 4MC (Fig. 5b). These findings also matched the EDX measurements.

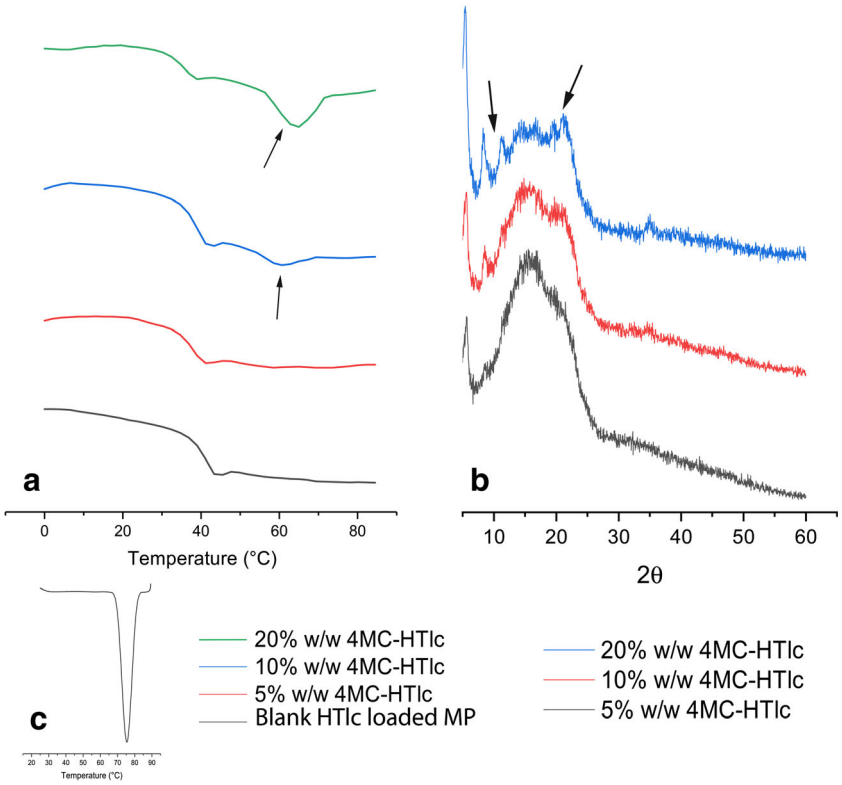

Fig. 5 **a** Thermal and **b** XRPD profiles of the 4MC-sHTC loaded MP. **c** Insert of the 4MC thermal profile

Such observations suggest that a small amount of 4MC may be released from the intercalation compound during preparation, a phenomenon likely due to a partial contact of the dispersed 4MC-sHTC solid with the organic solvent upon emulsification.

The above observations were confirmed by measuring the release of 4MC over 30 days (Fig. 6). In fact, at 20% *w/w* loading, 4MC was almost completely released within the first week from the 4MC-sHTC-loaded MP. This behavior could be explained by considering the higher inner porosity, the higher localization of the intercalation compound near the particle surface, as well as the presence of traces of free 4MC, as suggested by the DSC and XRPD analyses.

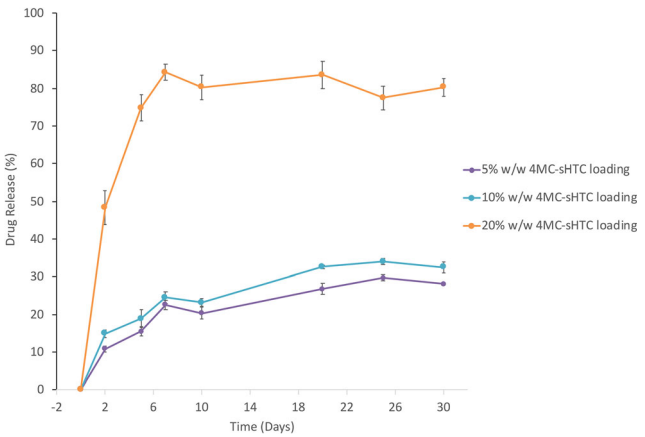

Fig. 6 In vitro release profiles of the 4MC-sHTC loaded R202S MP over a 30-day period. The experiment was performed in triplicate in 30% *w/v* PEG400, 0.1 M phosphate buffer pH 7.4 at 37 °C

At lower loadings, only 25–30% of 4MC was released over 30 days. Compared with the profiles obtained for the 4MC-loaded R202S MP, the use of sHTC seemed to allow extension of the release for a longer period of time. It should be minded that the low profile of the 20% *w/w* 4MC-loaded R202S MP was due to particle aggregation and formation of large clumps with loss of particle morphology. On the contrary, the slow release observed for the 4MC-sHTC-loaded MP is the likely result of a better entrapment of the molecule in the particle core and a higher glassy state of the polymer matrix.

The investigation of the possible release mechanism from the MP was carried out as already described for the 4MC-loaded MP. Even in this case, the best fitting model was the Peppas' that was therefore employed to theorize the most probable release mechanism.

The n estimates reported in Table 5 suggest that a pure Fickian transport is the dominant process leading to 4MC release ($0.12 < n < 0.32$) at all loadings. Therefore, the use of sHTC determined mainly a diffusional release process with an evident contribution of the higher inner porosity [57]. Overall, it is clear that the intercalation in the sHTC clay decreased the impact of 4MC loading on the MP physical state thus potentially reducing the issues hindering MP manufacturing and storage.

Table 5 Fitting of zero-order, Higuchi's, and Peppas' models to 4MC in vitro release data from R202S MP loaded with the 4MC-sHTC inclusion compound

Model	Zero order		Higuchi		Peppas		
% *w/w* loading	Adj. r^2	Red. χ^2	Adj. r^2	Red. χ^2	Adj. r^2	Red. χ^2	$n \pm$ (SE)
5	0.29612	71.63	0.87003	13.23	0.95858	4.22	0.32 ± 0.05
10	0.23766	99.96	0.86092	18.24	0.97501	3.28	0.30 ± 0.03
20	0.92165	1628.24	0.22508	656.60	0.90815	77.82	0.12 ± 0.05

Adjusted r^2 r^2 adjusted for the number of predictor terms in the model, *Reduced* χ^2 χ^2/DoF as obtained by the Levenberg-Marquardt method

Storage Stability of 4MC and 4MC-sHTC-Loaded MP

In order to establish whether the sHTC strategy may improve MP storage stability, the 20% *w/w* 4MC and 4MC-sHTC-loaded MP batches were maintained for 8 months at controlled temperature and humidity. Thermal and XRPD analyses as well as morphological observations were then replicated.

In Fig. 7, the 4MC-loaded MP preserved their round shape; however, a significant increase of aggregates was observed for almost all batches (Fig. 7a–d, f). Only the PDLG7507 MP appeared less clumped although with an increase of surface crystals, likely ascribable to 4MC. Aggregation was due to polymer annealing that softened the polymer matrix over time and favored particle fusion and adhesion.

On the other hand, the 4MC-sHTC-loaded R202S MP were practically unchanged. The 20% *w/w* 4MC-loaded R202S MP were not included in this study as their structure and morphology were already lost shortly after preparation.

The XRPD profiles after 8 months of incubation showed a small increase of crystallinity for some batches, such as the RG504H, PDLG5004A MP, and, to a lower extent, the PDLG75057 MP (Fig. 7). These modifications can be due to a slow tendency of 4MC to recrystallize and segregate, which can become a considerable issue over long-term storage of such formulations. The R202S MP loaded with 4MC-sHTC were almost identical, with profiles showing small peaks not corresponding to the main 4MC signals.

The profile alterations highlighted in Fig. 7 were partially confirmed by the measurement of T_g changes on the aged batches. Significant T_g variations were recorded for the RG504H, PDLG7505, RG504, and PDLG5004A MP, nearly in line with the observed slight changes in crystallinity (Fig. 8a). In addition, the DSC profiles also showed an increase in the melting signal of 4MC almost in all the mentioned batches (Fig. 8b).

Non-significant T_g shifts were instead measured for the RG502 and R202S MP loaded with the intercalation compound.

These observed changes could be the result of a reorganization of 4MC distribution in the polymer matrix. If slow crystallization occurs, a concerted T_g increase is expected due to segregation of crystals that give rise to a new physical phase, reducing the amount of active molecularly dispersed in the polymer matrix. In turn, if additional solubilization occurs, further T_g depletion may be recorded.

Such events could correspond to those observed in Fig. 8, where the T_g increase measured for the RG504H MP and, to a much smaller extent, for the RG504 and PDLG5004A MP reflects a possible 4MC crystallization and segregation, partially confirmed by the XRPD profiles (Fig. 7). On the contrary, no significant changes of the 4MC-sHTC distribution in the MP was observed by EDX (Fig. 8c). In all cases, the behavior observed was consistent with that of the freshly prepared MP.

Conclusions

The two distinct steps performed were useful to address manufacturing issues of the newly formulated 4MC-loaded PLA and PLGA MP and to evaluate the proposed new stabilization strategy. The considerable plasticization induced by 4MC entrapment arose serious problems upon MP manufacturing and storage, confirming the predictable effect that small plasticizing molecules can exhibit on low glassy polymeric matrices. In particular, the extensive effect on the 4MC-loaded R202S MP prevented recovery and storage.

The formation of the 4MC-sHTC intercalation complex proposed as a proof of concept stabilization strategy was successful in improving MP manufacturing and storage stability. Although this approach was tested only on the most problematic batch, the results obtained could be reasonably extended to all similar PLA and PLGA MP. The assumption that the entrapment of 4MC in the modified clay would have limited the interaction with the polymer was confirmed by the increased stability upon fabrication and 8-month storage. Therefore, this strategy is surely worth of further investigation in order to be transferred to other MP drug delivery systems.

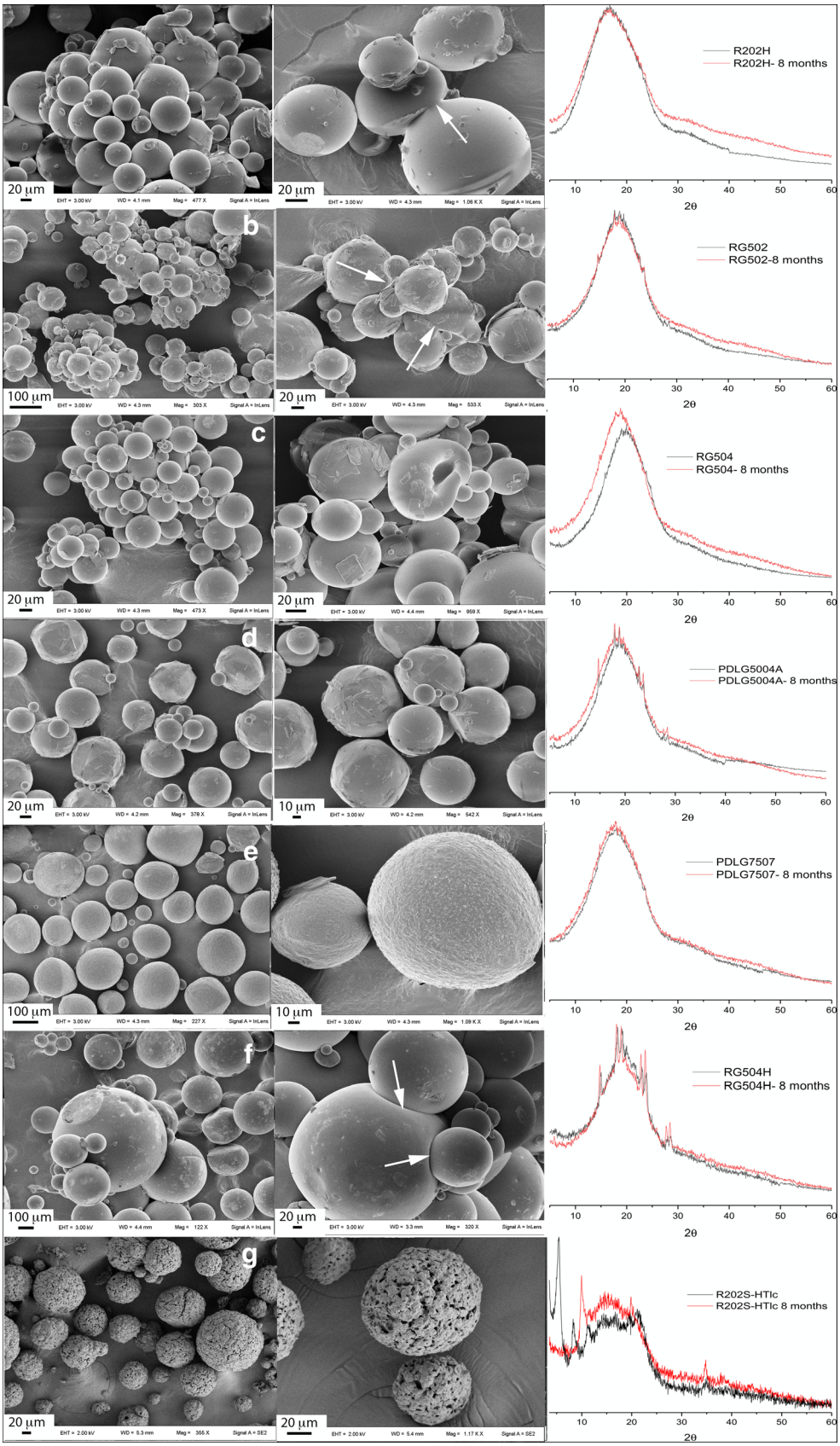

Fig. 7 Morphology of the 20% *w/w* 4MC and 4MC-sHTC-loaded MP after storage for 8 months at rt and 30% RH. **a** R202H. **b** RG502. **c** RG504. **d** PDLG5004A. **e** PDLG7507. **f** RG504H. **g** 4MC-sHTC-loaded MP. Arrows = clusters and adhesion points among particles due to polymer annealing. Right = comparison of the corresponding XRPD profiles recorded before and after storage for 8 months at rt and 30% RH

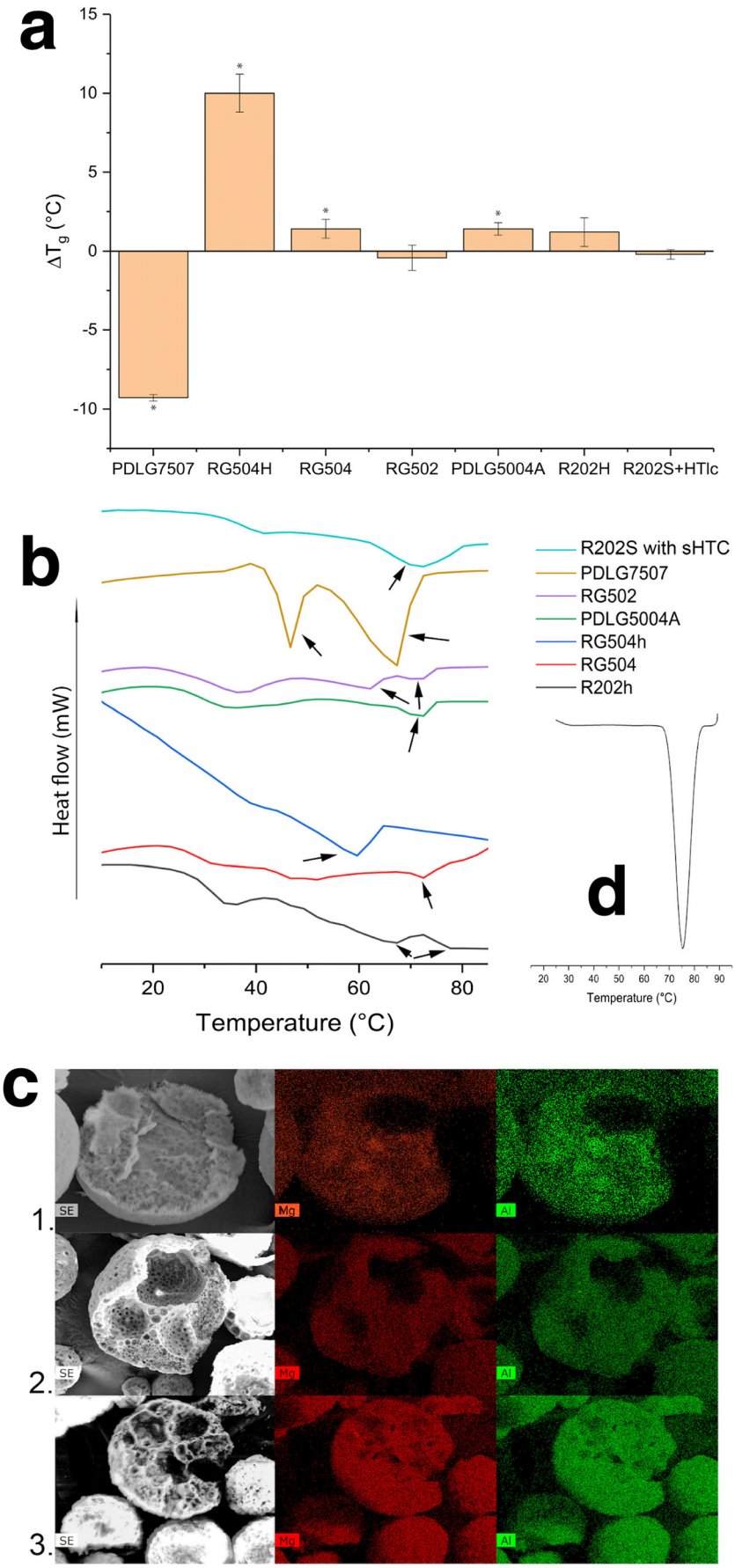

Fig. 8 Thermal and spectroscopic characterization of the 4MC and 4MC-sHTC loaded MP after storage for 8 months at rt and 30% RH. **a** T_g changes. **b** DSC profiles at 20% loading, arrows show 4MC melting, $*p < 0.05$. **c** EDX mapping of 4MC-sHTC in the MP at 1 = 5%, 2 = 10%, and 3 = 20% loading (red = Mg signal, green = Al signal). **d** Insert of the 4MC thermal profile

Funding information The authors are thankful to CAPES (PVE, grant 88887.116106/2016- 00) (Coordenação de Aperfeiçoamento de Pessoal de Nível Superior), Brazil, for providing financial support in the form of a doctoral's degree scholarship to Benvenutti, D. F. and to financial support (Science Program Without Borders—Researcher Special Visitor—PVE), CNPq (Conselho Nacional de Desenvolvimento Científico e Tecnológico, Edital Universal, grant 88887.122964/2016-00).

References

1. Zhuang C, Zhang W, Sheng C, Zhang W, Xing C, Miao Z. Chalcone: a privileged structure in medicinal chemistry. Chem Rev [Internet]. 2017;117:7762–810. Available from: http://pubs.acs.org/doi/10.1021/acs.chemrev.7b00020.
2. Nielsen SF, Boesen T, Larsen M, Schønning K, Kromann H. Antibacterial chalcones—bioisosteric replacement of the 4′-hydroxy group. Bioorg Med Chem. 2004;12:3047–54.
3. Pandhurnekar CP, Meshram EM, Chopde HN, Batra RJ. Synthesis, characterization, and biological activity of 4-(2-hydroxy-5-(aryldiazenyl)phenyl)-6-(aryl)pyrimidin-2-ols derivatives. Org Chem Int [Internet]. 2013;2013:1–10. Available from: https://www.hindawi.com/archive/2013/582079/.
4. De Carvalho Tavares L, Johann S, Maria De Almeida Alves T, Guerra JC, Maria De Souza-Fagundes E, Cisalpino PS, et al. Quinolinyl and quinolinyl N-oxide chalcones: synthesis, antifungal and cytotoxic activities. Eur J Med Chem. 2011;46:4448–56.
5. Lahtchev KL, Batovska DI, Parushev SP, Ubiyvovk VM, Sibirny AA. Antifungal activity of chalcones: a mechanistic study using various yeast strains. Eur J Med Chem. 2008;43:2220–8.
6. Trivedi JC, Bariwal JB, Upadhyay KD, Naliapara YT, Joshi SK, Pannecouque CC, et al. Improved and rapid synthesis of new coumarinyl chalcone derivatives and their antiviral activity. Tetrahedron Lett. 2007;48:8472–4.
7. Kaur K, Jain M, Reddy RP, Jain R. Quinolines and structurally related heterocycles as antimalarials. Eur J Med Chem. 2010. p. 3245–64.
8. Tomar V, Bhattacharjee G, Kamaluddin RS, Srivastava K, Puri SK. Synthesis of new chalcone derivatives containing acridinyl moiety with potential antimalarial activity. Eur J Med Chem. 2010;45:745–51.
9. Boeck P, Bandeira Falcão CA, Leal PC, Yunes RA, Filho VC, Torres-Santos EC, et al. Synthesis of chalcone analogues with increased antileishmanial activity. Bioorg Med Chem. 2006;14:1538–45.
10. Chen M, Zhai L, Christensen SB, Theander TG, Kharazmi A. Inhibition of fumarate reductase in Leishmania major and l. donovani by chalcones. Antimicrob Agents Chemother. 2001;45:2023–9.
11. Vogel S, Barbic M, Jürgenliemk G, Heilmann J. Synthesis, cytotoxicity, anti-oxidative and anti-inflammatory activity of chalcones and influence of A-ring modifications on the pharmacological effect. Eur J Med Chem. 2010;45:2206–13.
12. Yadav VR, Prasad S, Sung B, Aggarwal BB. The role of chalcones in suppression of NF-kappaB-mediated inflammation and cancer. Int Immunopharmacol [Internet]. 2011;11:295–309. Available from: http://www.pubmedcentral.nih.gov/articlerender.fcgi?artid=3058688&tool=pmcentrez&rendertype=abstract%5Cn, http://www.ncbi.nlm.nih.gov/pubmed/21184860.
13. Vijaya Bhaskar Reddy M, Tsai WJ, Qian K, Lee KH, Wu TS. Structure-activity relationships of chalcone analogs as potential inhibitors of ADP- and collagen-induced platelet aggregation. Bioorg Med Chem. 2011;19:7711–9.
14. Szliszka E, Czuba ZP, Mazur B, Paradysz A, Krol W. Chalcones and dihydrochalcones augment TRAIL-mediated apoptosis in prostate cancer cells. Molecules. 2010;15:5336–53.
15. Kachadourian R, Day BJ, Pugazhenti S, Franklin CC, Genoux-Bastide E, Mahaffey G, et al. A synthetic chalcone as a potent inducer of glutathione biosynthesis. J Med Chem. 2012;55:1382–8.
16. Ortolan XR, Mezadri TJ, Tames DR, Corrêa R, De Campos Buzzi F. Osteogenic potential of different chalcones in an in vivo model: a preliminary study. J Oral Res. 2017;6:209–15.
17. Ortolan XR, Fenner BP, Mezadri TJ, Tames DR, Corrêa R, De Campos Buzzi F. Osteogenic potential of a chalcone in a critical-size defect in rat calvaria bone. J Cranio-Maxillofac Surg. 2014;42:520–4.
18. Ramalho SD, Bernades A, Demetrius G, Noda-Perez C, Vieira PC, Dos Santos CY, et al. Synthetic chalcone derivatives as inhibitors of cathepsins K and B, and their cytotoxic evaluation. Chem Biodivers. 2013;10:1999–2006.
19. Lim J, Lee SH, Cho S, Lee IS, Kang BY, Choi HJ. 4-methoxychalcone enhances cisplatin-induced oxidative stress and cytotoxicity by inhibiting the Nrf2/ARE-mediated defense mechanism in A549 lung cancer cells. Mol Cells. 2013;36:340–6.
20. Dhanapal V, Gopinath C, Ashajothi B, Ramalingam J, Raman AN. A facile synthesis and the study of some new chacones for analgesic and anti-inflammatory activity. Am J Pharmtech Res. 2013;3:252–61.
21. Mattos CB, Deponti VB, Barreto F, Simões CMO, Andrighetti-Frohner CR, Nunes RJ, et al. Development of a stability-indicating LC method for determination of a synthetic chalcone derivative in a nanoemulsion dosage form and identification of the main photodegradation product by LC–MS. J Pharm Biomed Anal. 2012;70:652–6.
22. Wei Y, Wang Y, Kang A, Wang W, Ho SV, Gao J, et al. A novel sustained-release formulation of recombinant human growth hormone and its pharmacokinetic, pharmacodynamic and safety profiles. Mol Pharm. 2012;9:2039–48.
23. Tran VT, Karam JP, Garric X, Coudane J, Benoît JP, Montero-Menei CN, et al. Protein-loaded PLGA-PEG-PLGA microspheres: a tool for cell therapy. Eur J Pharm Sci. 2012;45:128–37.
24. Passerini N, Albertini B, Di Sabatino M, Corace G, Luppi B, Canistro D, et al. Development of microparticles for oral administration of the non-conventional radical scavenger IAC and testing in an inflammatory rat model. Int J Pharm. 2016;512:126–36.
25. Cambronero-Rojas A, Torres-Vergara P, Godoy R, Von Plessing C, Sepúlveda J, Gómez-Gaete C. Capreomycin oleate microparticles for intramuscular administration: preparation, in vitro release and preliminary in vivo evaluation. J Control Release. 2015;209:229–37.
26. Lu Z, Tsai M, Lu D, Wang J, Wientjes MG, Au JL-S. Tumor-penetrating microparticles for intraperitoneal therapy of ovarian Cancer. J Pharmacol Exp Ther [Internet]. 2008;327:673–82. Available from: http://jpet.aspetjournals.org/cgi/doi/10.1124/jpet.108.140095.
27. Mwangi TK, Bowles RD, Tainter DM, Bell RD, Kaplan DL, Setton LA. Synthesis and characterization of silk fibroin microparticles for intra-articular drug delivery. Int J Pharm. 2015;485:7–14.
28. Giovagnoli S, Palazzo F, Michele A Di, Schoubben A, Blasi P, Ricci M. The influence of feedstock and process variables on the encapsulation of drug suspensions by spray-drying in fast drying regime: the case of novel antitubercular drug–palladium complex containing polymeric microparticles. J Pharm Sci [Internet]. 2014;103:1255–68. Available from: http://linkinghub.elsevier.com/retrieve/pii/S0022354915306481.
29. Takenaga M, Serizawa Y, Azechi Y, Ochiai A, Kosaka Y, Igarashi R, et al. Microparticle resins as a potential nasal drug delivery system for insulin. J Control Release. 1998;52:81–7.
30. Huang J, Wigent RJ, Schwartz JB. Drug-polymer interaction and its significance on the physical stability of nifedipine amorphous dispersion in microparticles of an ammonio methacrylate copolymer and ethylcellulose binary blend. J Pharm Sci. 2008;97:251–62.
31. Blasi P, Schoubben A, Giovagnoli S, Perioli L, Ricci M, Rossi C. Ketoprofen poly(lactide-co-glycolide) physical interaction. AAPS

PharmSciTech [Internet]. 2007;8:Article 37. Available from: http://www.pubmedcentral.nih.gov/articlerender.fcgi?artid=2750376&tool=pmcentrez&rendertype=abstract.
32. Giovagnoli S, Blasi P, Ricci M, Rossi C. Biodegradable microspheres as carriers for native superoxide dismutase and catalase delivery. AAPS PharmSciTech [Internet]. 2004;5:1–9. Available from: http://www.springerlink.com/index/10.1208/pt050451.
33. Giovagnoli S, Blasi P, Ricci M, Schoubben A, Perioli L, Rossi C. Physicochemical characterization and release mechanism of a novel prednisone biodegradable microsphere formulation. J Pharm Sci [Internet]. 2008;97:303–17. Available from: http://linkinghub.elsevier.com/retrieve/pii/S002235491632439X.
34. Giovagnoli S, Blasi P, Schoubben A, Rossi C, Ricci M. Preparation of large porous biodegradable microspheres by using a simple double-emulsion method for capreomycin sulfate pulmonary delivery. Int J Pharm. 2007;333:103–11.
35. Makris EA, Gomoll AH, Malizos KN, Hu JC, Athanasiou KA. Repair and tissue engineering techniques for articular cartilage. Nat Rev Rheumatol [Internet]. 2015;11:21–34. Available from: http://www.nature.com/articles/nrrheum.2014.157.
36. Chung HJ, Park TG. Surface engineered and drug releasing prefabricated scaffolds for tissue engineering. Adv Drug Deliv Rev [Internet]. 2007;59:249–62. Available from: http://linkinghub.elsevier.com/retrieve/pii/S0169409X07000270.
37. Makadia HK, Siegel SJ. Poly lactic-co-glycolic acid (PLGA) as biodegradable controlled drug delivery carrier. Polymers (Basel). 2011;3:1377–97.
38. Kalogeras IM. A novel approach for analyzing glass-transition temperature vs. composition patterns: application to pharmaceutical compound + polymer systems. Eur J Pharm Sci. 2011;42:470–83.
39. Albertini B, Iraci N, Schoubben A, Giovagnoli S, Ricci M, Blasi P, et al. β-cyclodextrin hinders PLGA plasticization during microparticle manufacturing. J Drug Deliv Sci Technol [Internet]. 2015;30:375–83. Available from: http://linkinghub.elsevier.com/retrieve/pii/S1773224715001392.
40. Costantino U, Nocchetti M, Sisani M, Vivani R. Recent progress in the synthesis and application of organically modified hydrotalcites. Zeitschrift für Krist [Internet]. 2009;224. Available from: http://www.degruyter.com/view/j/zkri.2009.224.issue-5-6/zkri.2009.1153/zkri.2009.1153.xml.
41. Corrêa R, Pereira MAS, Buffon D, dos Santos L, Filho VC, Santos ARS, et al. Antinociceptive properties of chalcones. Structure-activity relationships. Arch Pharm (Weinheim) [Internet]. 2001;334:332–4. Available from: http://doi.wiley.com/10.1002/1521-4184%28200110%29334%3A10%3C332%3A%3AAID-ARDP332%3E3.0.CO%3B2-O
42. Costantino U, Gallipoli A, Nocchetti M, Camino G, Bellucci F, Frache A. New nanocomposites constituted of polyethylene and organically modified ZnAl-hydrotalcites. Polym Degrad Stab. 2005;90:586–90.
43. Higuchi T. Rate of release of medicaments from ointment bases containing drugs in suspension. J Pharm Sci. 1961;50:874–5.
44. Ritger PL, Peppas NA. A simple equation for description of solute release I. Fickian and non-fickian release from non-swellable devices in the form of slabs, spheres, cylinders or discs. J Control Release. 1987;5:23–36.
45. Kosmidis K, Rinaki E, Argyrakis P, Macheras P. Analysis of case II drug transport with radial and axial release from cylinders. Int J Pharm. 2003;254:183–8.
46. Levenberg K. A method for the solution of certain non-linear problems in least squares. Q J Appl Math. 1944;2:164–8.
47. Marquardt DW. An algorithm for least-squares estimation of nonlinear parameters. J Soc Ind Appl Math [Internet]. 1963;11:431–41. Available from: http://epubs.siam.org/doi/10.1137/0111030.
48. Wischke C, Schwendeman SP. Principles of encapsulating hydrophobic drugs in PLA/PLGA microparticles. Int J Pharm [Internet]. 2008;364:298–327. Available from: http://linkinghub.elsevier.com/retrieve/pii/S0378517308003517.
49. Allison SD. Effect of structural relaxation on the preparation and drug release behavior of poly(lactic-co-glycolic)acid microparticle drug delivery systems. J Pharm Sci [Internet]. 2008;97:2022–35. Available from: http://linkinghub.elsevier.com/retrieve/pii/S0022354916325746.
50. Alexis F. Factors affecting the degradation and drug-release mechanism of poly(lactic acid) and poly[(lactic acid)-co-(glycolic acid)]. Polym Int [Internet]. 2005;54:36–46. Available from: http://doi.wiley.com/10.1002/pi.1697.
51. Tracy MA, Ward KL, Firouzabadian L, Wang Y, Dong N, Qian R, et al. Factors affecting the degradation rate of poly(lactide-co-glycolide) microspheres in vivo and in vitro. Biomaterials. 1999;20:1057–62.
52. Fredenberg S, Wahlgren M, Reslow M, Axelsson A. The mechanisms of drug release in poly(lactic-co-glycolic acid)-based drug delivery systems—a review. Int J Pharm. 2011;415:34–52.
53. Kang J, Schwendeman SP. Pore closing and opening in biodegradable polymers and their effect on the controlled release of proteins. Mol Pharm. 2007;4:104–18.
54. Huang J, Mazzara JM, Schwendeman SP, Thouless MD. Self-healing of pores in PLGAs. J Control Release. 2015;206:20–9.
55. Siepmann J. Modeling of drug release from delivery systems based on hydroxypropyl methylcellulose (HPMC). Adv Drug Deliv Rev [Internet]. 2001;48:139–57. Available from: http://linkinghub.elsevier.com/retrieve/pii/S0169409X01001120.
56. Ritger PL, Peppas NA. A simple equation for description of solution release I. frickian and non-frickian release from non-sweliable devices in the form of slabs,spheres,cylinders or discs. J Control Release. 1987;5:23–36.
57. Klose D, Siepmann F, Elkharraz K, Krenzlin S, Siepmann J. How porosity and size affect the drug release mechanisms from PLGA-based microparticles. Int J Pharm. 2006;314:198–206.